Journal of Asian Earth Sciences 78 (2013) 263–276

Contents lists available at SciVerse ScienceDirect

Journal of Asian Earth Sciences

journal homepage: www.elsevier.com/locate/jseaes

Geophysical evidence on segmentation of the Tancheng-Lujiang fault and its implications on the lithosphere evolution in East China

Yangfan Deng [a,b,c,*], Weiming Fan [a], Zhongjie Zhang [c], José Badal [d]

[a] Guangzhou Institute of Geochemistry, Chinese Academy of Sciences, Guangzhou 510640, China
[b] University of Chinese Academy of Sciences, Beijing 100049, China
[c] State Key Laboratory of Lithospheric Evolution, Institute of Geology and Geophysics, Chinese Academy of Sciences, Beijing 100029, China
[d] Physics of the Earth, University of Zaragoza, Pedro Cerbuna 12, 50009 Zaragoza, Spain

ARTICLE INFO

Article history:
Available online 15 November 2012

Keywords:
P-wave velocity
Seismicity
Crustal rheology
Geothermal field
Segmentation properties
Tanlu fault

ABSTRACT

The north–south trending Tancheng-Lujiang (Tanlu) fault belt extends from northeast China to the Dabie–Sulu orogenic belt, for a length of more than 3000 km. This fault belt probably has close links with the lithosphere evolution, seismic activity and mineral resource concentration in East China. Surface geological mapping and studies on sedimentation and basin formation have indicated segmentation at the southern, middle and northern domains of the fault. Here we employ geophysical constraints to evaluate these fault segments. Unlike previous geophysical studies focused on laterally varying crust/mantle seismic velocity structure across the fault, in this study we have integrated a variety of geophysical data sets, such as crustal P-wave velocity, earthquake occurrence and released seismic energy, seismogenic layer thickness, surface heat flow and geothermal field, to understand the deep structure and strength of the lithosphere along the Tanlu segmented fault belt. The results demonstrate remarkable crustal-scale north-to-south segmentation this major fault. The geophysical evidence and some geochemical constraints suggest that the Tanlu fault belt probably served as a channel for melt and fluid percolation, and exerted a significant control on the lithosphere evolution in East China.

1. Introduction

The Tancheng-Lujiang fault belt, also known as Tanlu fault or by its acronym TLF, with a length greater than 3000 km, extends north–northeast along the eastern margin of mainland China. The faults trends from the Songliao basin (Heilongjiang Province) in the north to Lujiang (Anhui Province) of the Dabie–Sulu orogenic belt, through the Bohai Sea (Salon, 1977; Xu, 1984b; Xu et al., 1987; Li et al., 1994; Wan et al., 1996; Teng et al., 2001, 2006; Zhu et al., 2002, 2004; Bai et al., 2007; Martin et al., 2007; Zhang et al., 2007) (Fig. 1). The Tanlu fault and the San Andreas fault are the two important tectonic belts on both western and eastern margins of the Pacific Ocean (Mount and Suppe, 1987). Numerous geological, tectonic and geochemical studies suggest that TLF has undergone multistage structural deformations since the Mesozoic, thus showing quite different properties during different periods, such as left-lateral strike slip in the Early Cretaceous, extensional deformation during the Late Cretaceous and Paleogene, and compression and right-lateral strike slip since the Neogene (Wan et al., 1996; Zhu et al., 2004). Various mechanisms have been proposed to explain the formation of TLF. An early proposal explained that TLF is part of a wide wrench fault system along the northeastern Asian continent and that sinistral displacement along this fault system accommodated oblique convergence between the Pacific oceanic plate and the Asian continent (Xu et al., 1987, 1993; Zhu et al., 2004), as also is argued in more recent studies based on seismic observation (Tian et al., 2009; Zhao et al., 2009a,b; Chen, 2010). Yin and Nie (1993) and then Li (1994) considered that TLF formed as a result of the collision between the North and South China Blocks during the Late Triassic and that the fault was strongly activated during the Cretaceous and Cenozoic periods (Fan and Menzies, 1992; Fan et al., 2000, 2007; Zhao et al., 2009a,b). It has been also suggested that TLF belongs to the rift system of eastern China (Xu et al., 1987; Xu and Zhu, 1995; Hsiao et al., 2004). Regionally, Cenozoic tectonics in north China is characterized by widespread rifting and extension, which caused the formation of petroliferous basins, such as the Bohai Sea and Yellow Sea (Ma and Wu, 1987). Furthermore, Li et al. (2012a,b) considered that different patterns of the basins on both sides of the TLF were controlled by escape tectonics in different domains of the crust. It is generally considered that Tertiary rifting and extension in the

* Corresponding author at: Guangzhou Institute of Geochemistry, Chinese Academy of Sciences, Guangzhou 510640, China.
E-mail addresses: dengyangfan@mail.iggcas.ac.cn (Y. Deng), zhangzj@mail.iggcas.ac.cn (Z. Zhang).

1367-9120/$ - see front matter © 2012 Elsevier Ltd. All rights reserved.
http://dx.doi.org/10.1016/j.jseaes.2012.11.006

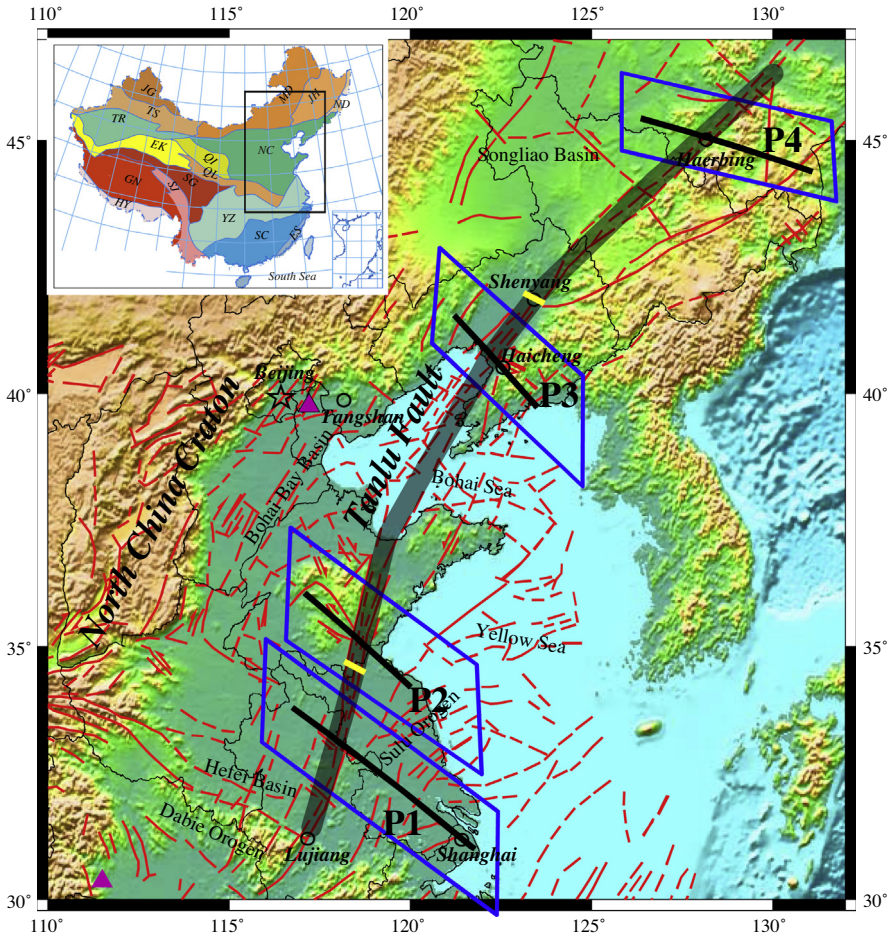

Fig. 1. Schematic representation of TLF across East China. The involved region is outlined by a rectangle drawn on a map of China (top left inset). Discontinuous lines depict the fault zones, while TLF is drawn with a translucent thick line. Linear segments of thick stroke represent the positions of four wide-angle seismic profiles crossing TLF: Fuliji–Fengxian (P1), Lianyungang-Sishui (P2), Yixian–Youyan (P3) and Haerbing–Suifenhe (P4). Counting of earthquakes and computation of the seismic energy released has been made inside the areas delimited by quadrilaterals. Two very short thick yellow strokes upon TLF delimit the segmented structure of the fault; while two triangles mark the positions NCC and SC mentioned in Fig. 7.

North China Craton (NCC) resulted from back-arc spreading of the mantle induced by westward subduction of the Pacific plate beneath the Asian continent, resulting the destruction and significant lithospheric thinning of the eastern NCC (Uyeda and Miyashiro, 1974; Uyeda and Kanamori, 1979; Ye et al., 1987; Yang et al., 2011, 2012; Zhai and Santosh, 2011; Zhang et al., 2012a,b; Zhu et al., 2012). Moreover, the presence of active faults in north China and the strong earthquake occurrences, such as the 1668 Mw 8.5 Shandong earthquake and the 1975 Mw 7.3 Haicheng earthquake, show that dextral slip occurred along the Tanlu fault zone during the Quaternary, which is associated with eastward extrusion of the South China Block as a consequence of the late-stage India-Eurasia convergence (Tapponnier and Molnar, 1977; Peltzer et al., 1985; Zhang et al., 1995, 1998), or with transpression at the southern and northern margins of the NCC (Zhang et al., 2003a,b) accompanied by the northward and southward extrusions of the lower crust (Zhang et al., 2011d). The mechanism of formation of TLF is still under dispute.

Owing to its intrinsic complexity, the occurrence of destructive earthquakes and the existence of rich mineral deposits (Teng et al., 1983), TLF initially raised the interest of the Ministry of Geology (now the Ministry of Geology and Mineral Resources) that sponsored an aeromagnetic survey in the 1950s with the obvious aim of exploring possible mineral resources (Wan et al., 1996; Zhang and Zhang, 2007). From then, several institutions including the Chinese Academy of Sciences, Ministry of Lands and Resources, China Earthquake Administration and also some universities have carried out various geological, geochemical and geophysical studies related to TLF. Several wide-angle seismic profiles (Zheng and Teng, 1989; Yang et al., 1996; Bai et al., 2007), nearly vertical seismic reflection surveys in Bohai Bay basin, Liaodong Bay (Hsiao et al., 2004) and Jiangsu Province (Chen et al., 1999), and magneto-telluric soundings (Ye et al., 2009; Zhang et al., 2010b) were also carried out. Many of the results from the wide-angle seismic profiles (mainly focused on lateral variations across TLF) were published in Chinese journals and books (Ma et al., 1991; Lu and Xin, 1993; Fu and Yang, 1998; Deng et al., 2011), and these data set provide valuable information (Li et al., 2006a; Zhang et al., 2011c, 2012b).

In this study, we have analyzed four profiles that intersect TLF almost normally and obliquely at different latitudes by integrating different data sources, namely: wide-angle seismic data, spatial distribution of the seismicity, surface heat flow and geothermal field. We have paid special attention to the lateral variation of the crustal thickness, released seismic energy and lithosphere rheology, average P-wave velocity of the seismogenic crustal layers, and temperature distribution in the crust and uppermost mantle. Based on this information, we have presented the segmentation properties of TLF, discussed possible mechanisms and implications on the lithosphere evolution in East China.

2. Tectonic evidence on the segmentation of TLF

The TLF is assumed as a large active lithospheric fault running through the eastern margin of the Pacific region of China. It strikes in N30°E (Xu, 1984a,b) and plays a decisive role on the regional structure, sedimentary paleogeography, magmatism, distribution of mineral deposits and seismic activity in East China (Xu et al., 1993; Xu and Zhu, 1995; Wu et al., 2005; Xiao et al., 2010). Several studies demonstrate that the fault was disintegrated into various segments by fractures in NW–SE direction. Remarkable differences can be seen in the mode and direction of the activities; for instance a rough demarcation can be made at Shenyang, where small magnitude extension dominated in its north segment, whereas alternation of dextral compressional shearing and extensional rifting was predominant in the south (Wang et al., 1998).

A number of sedimentary basins occur along the TLF; from north to south these are: Sanjiang (Three Rivers), Songliao, Yilan-Yitong, Liaoxi, Bohai Bay, Jiaolai (Jiaozhouwan-Lauhouwan), Luxi, Yishu, Subei, Hefei and Jianghan (Zhu et al., 2001b; Li et al., 2012b; Scott et al., 2012). Large basins such as the Songliao and the Subei-Yellow Sea basins, that are rich in oil and gas resources, are located on both sides of the fault belt or within the fault zone. All the basins crossed by the TLF system have experienced three stages of mantle uplifting, lithospheric extension-rift faulting, and compression. The first one was the compression-shearing stage of TLF; the second the rifting stage, which also was the formation stage of the source rocks; and the third was that of petroleum generation, migration and accumulation by compression-shearing of TLF (Wang et al., 1998).

Below we briefly summarize the geophysical and geological data bearing on the origin of segmentation of the TLF. Gravity and magnetic anomalies extend in the southern part of the fault (Jiangsu and Anhui Province) in NW–SE direction. Here the fault belt consists of several obliquely arranged faults and the dominant sedimentation includes Cretaceous, Palaeogene and Neogene formations (Zhang and Zhang, 2007). Studies on the structure and sedimentation have demonstrated that sinistral strike-slip movement dominated in this part during the Early Cretaceous, responsible for the eruptive activity and the large-scale intrusion of volcanic rocks and strong mylonitization (Zhu et al., 2001a, 2005; Hou et al., 2003). An extensional movement featured the period between the Late Cretaceous and the Paleogene; the faults in the Hefei basin change their nature from compression to extension as revealed by nearby coarse clastic sedimentary rocks in the basin (Chen et al., 2004). Besides, the deep structure represents a remarkable compressional feature as revealed by a magnetotelluric sounding (Li et al., 2006b).

The middle segment (from Shandong Province to Shenyang, Liaoning Province) can be divided into two sub-segments. A slip movement in the southernmost part (Shandong Province) during the Early Cretaceous controlled the large-scale volcanism of Qingshan formation; in the Late Cretaceous the fault shows extensional movement with a thick succession of clastic sedimentary rock (Zhu et al., 2001b). The gravity and magnetic anomalies show a predominant NW to NE orientatin (Zhang et al., 2007). The northernmost part (from Bohai Bay to Shenyang) consists of series of NNE faults, and the sedimentation belongs to Cretaceous and Neogene. Between Triassic and Jurassic, NE and NW trending folds and thrust faults developed in the Bohai Bay basin, thus suggesting possible sinistral strike-slip displacement through NW–SE compression. In the Late Cretaceous, the fault in this part was in a compression state. The gravity and magnetic anomalies show NE direction (Zhang et al., 2007).

Finally, the northern segment (north of Shenyang, towards Jilin Province) formed between Early Cretaceous and Late Cretaceous, at around 100–95 Ma, with the simultaneous formation of a big lake (Qingshankou formation), thus suggesting a genetic relationship with the Songliao basin (Dou et al., 1996).

3. Seismic velocity structure as derived from wide-angle seismic profiles

As part of the national program in the frame of the Global Geosciences Transects (GGT) Project developed in the 80s, stimulated by the succession of disastrous earthquakes occurred in North China during the last few decades, numerous wide-angle seismic experiments were carried out in the east of continental China (Li et al., 2006a; Zhang et al., 2011c). Among these, there are four wide-angle seismic profiles (P1 to P4 in Fig. 1) crossing TLF along its southernmost segment (P1), central part (P2 and P3) and northern segment (P4), namely: (1) Fuliji–Fengxian profile (P1) (Bai et al., 2007); (2) Lianyungang-Sishui profile (P2) (Li, 1991; Ma et al., 1991); (3) Yixian–Youyan profile (P3) (CEA, 1992; Lu and Xin, 1993); (4) Haerbing–Suifenhe profile (P4) (Fu and Yang, 1998). Crustal velocity models related to these profiles were obtained by applying standard schemes (Ma, 1989; Li et al., 2006a; Zhang et al., 2011c), including picking up phases, ray-tracing and depth-to-layer inversion. Below, assuming a division of the crust into upper, middle and lower crust, we have summarized the results on layer depths and seismic velocities related to these reference profiles. Fig. 2 illustrates the topographic reliefs (data based on GTOPO30, top panels a, b, c and d) of each of these profiles and the corresponding crustal P-wave velocity models (bottom panels).

Profile 1 extends from Fuliji to Fengxian across the southern segment of TLF over a length of 570 km and a rough longitude range of 116–122°E (Fig. 2a), and was conducted by the ex-State Seismological Bureau (now Chinese Earthquake Administration) in 1984 (Bai et al., 2007). From the corresponding crustal P-wave velocity model (lower panel of Fig. 2a), we can observe 3–4 km Moho uplift beneath TLF (118°E), since the Moho depth varies between 31–33 km beneath TLF and 35 km beneath the Yangtze Block. Another notable finding is that the sediments are not thicker beneath the Hefei basin (2 km), but rather beneath the western of the Yangtze Block (5 km), when taking the P-wave velocity contour line of 6.0 km/s as the crystalline basement along the profile. The crustal P-wave velocity structure can be summarized as 5.6–6.2 km/s in the upper crust (at depths ranging from 0 to about 13 km), 6.2–6.5 km/s in the middle crust (extending from the bottom of the upper crust down to a depth of 25 km), and 6.6–7.1 km/s in the lower crust (down to a depth of about 35 km). The subcrustal P-wave velocity is usually taken as a reference to ascertain the thermal state of the topmost mantle (Wang et al., 2001; Xu et al., 2010); this seismic velocity can be estimated from the Pn phase (refracted wave from the topmost upper mantle) observed in wide-angle seismic experiments (Zhang et al., 2000, 2011c; Wang et al., 2000; Teng et al., 2006; Li et al., 2006a) or teleseismic Pn tomography (Liang et al., 2004; Huang and Zhao, 2006). In the China continent, the upper mantle velocities are usually 8.0 ± 0.2 km/s (Li et al., 2006a). However, the P-wave velocity estimated from the wide-angle seismic Pn phase recorded in the profile (118.5°E) reaches up to 8.3 km/s at the topmost mantle, which is much higher than the global average, thus indicating that the mantle should be colder beneath this region.

Profile 2 extends from Lianyungang (Jiangsu Province) to Sishui (Shandong Province) across the middle segment of TLF over a length of about 350 km, and through the Luxi Block with high elevation, Tanlu fault and Sulu orogeny belt with low elevation (Li, 1991). The most remarkable feature of the crustal velocity model (lower panel of Fig. 2b) is that the Moho topography remains flat

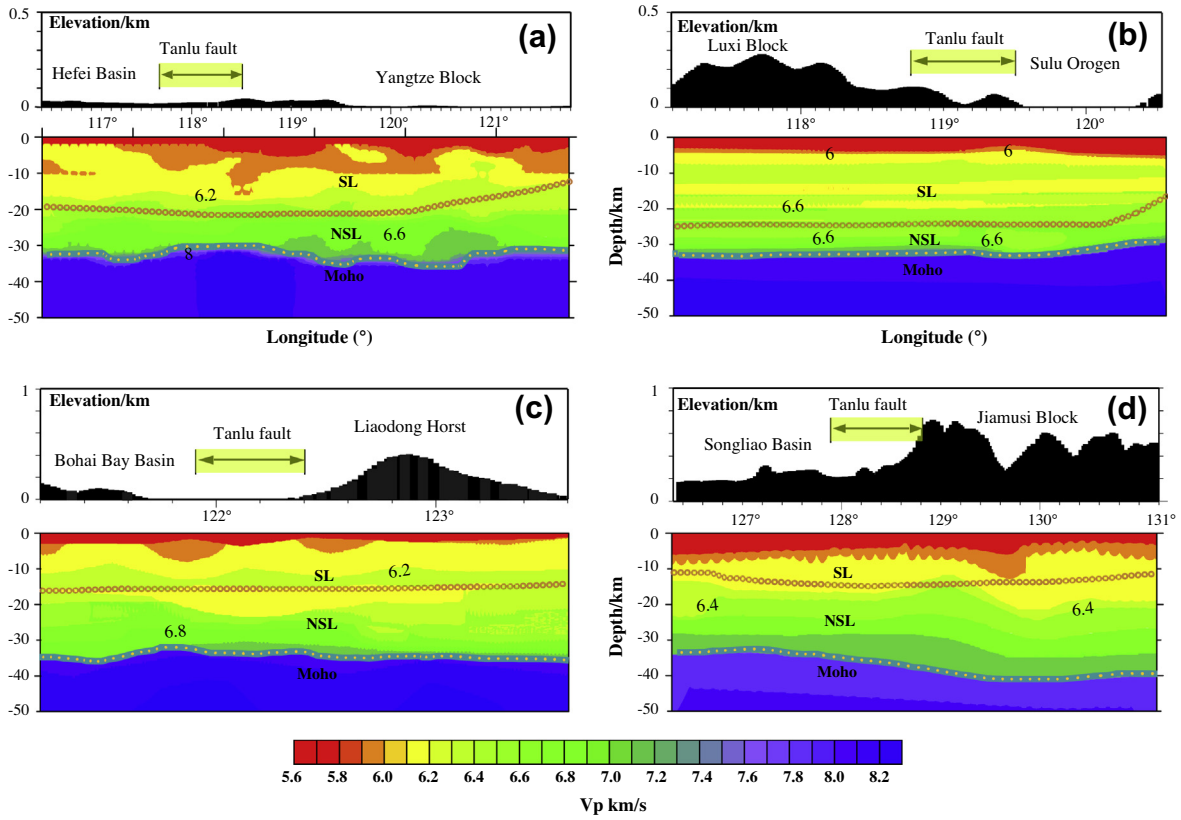

Fig. 2. Topographic reliefs (data based on GTOPO30, top panels a, b, c and d) and crustal P-wave velocity models (bottom panels) for the reference profiles (P1 to P4 in Fig. 1). SL means seismogenic layer wherein the 80% of the seismic energy is released and NSL means non-seismogenic layer (above the Moho discontinuity). On top of all graphs, the intersection of TLF (East China) with each reference profile is marked by arrows delimiting a gap in geographic longitude.

at 33 km depth beneath the Luxi Block (about 118°E), is a little undulation under TLF (119°E), and uplifts about 3 km beneath the Sulu orogeny (120°E), what is confirmed by receiver function migration (Chen et al., 2006) and seismic velocity profiles too (Bai et al., 2007). There is a well-developed flat layering in the crust beneath Luxi and Tanlu. The crustal P-wave velocity varies between 5.6 and 6.4 km/s in the upper crust (above 13 km roughly), from 6.0 to 6.5 km/s in the middle crust (to a depth of about 23 km), and from 6.5 to 7.4 km/s in the lower crust (down to a depth of about 33 km).

As part of the Dong-Ujimqinqi-Neimogol-Donggou Geoscience Transect, profile 3 extends from Yixian to the seismic zone of Haicheng (Liaoning Province) located in the North China Craton (Lu and Xin, 1993), across the central segment of TLF over a length of about 270 km (Fig. 2c). From the crustal velocity model (lower panel of Fig. 2c), we can observe that the Moho rises 3–4 km up to 31 km depth under TLF (122°E), but remains flat at 35 km depth beneath Liaodong Horst (123°E). The crustal P-wave velocity ranges from 5.6 to 6.3 km/s in the upper crust (about 16 km thick), between 6.1 and 6.6 km/s in the middle crust (to a depth of about 26 km), and between 6.6 and 7.0 km/s in the lower crust (down to a depth of about 33 km). A low velocity layer can be observed in the middle crust south of the Haicheng region.

As part of the Manzhouli–Suifenhe Geoscience Transect, profile 4 extends from the Songliao basin to the Jiamusi Block in Heilongjiang Province across the north segment of TLF over a length up to 400 km (Fig. 2d) (Yang et al., 1996; Fu and Yang, 1998). The surface topography and the Moho discontinuity show a typical image of symmetry (Zhang et al., 2011c): this interface is about 35 km depth under the Songliao basin and TLF (127–129°E), but the Moho sinks to about 41 km beneath the Jiamusi Block (130°E) in coincidence with a high elevation of the surface topography (lower panel of Fig. 2d). The crustal P-wave velocity values become progressively larger with increasing depth: 5.6–6.2 km/s in the upper crust (above 18 km approximately), 6.3–6.5 km/s in the middle crust (extending to a depth of 30 km), and 6.8–7.2 km/s in the lower crust, whose bottom reveals an undulated Moho.

4. Seismicity and crustal rheology

The lithospheric strength provides tighter constraints on its evolution, so that it can be used to understand the potential segmentation mechanism of TLF. The lithospheric strength can be expressed through isostasy and flexural rigidity (Watts, 2001), effective elastic thickness (Maggi et al., 2000; Audet et al., 2007; Pérez-Gussinyé et al., 2007, 2009), seismic activity and stress state (Ge and Zhang, 2009), seismicity and long-term rheology (Ranalli, 1997; Burov and Watts, 2006; Burov, 2010), and seismogenic layer thickness (Watts and Burov, 2003; Panza and Raykova, 2008; Zhang et al., 2010b, 2011c,e, 2012a,b). Given the difficulties to deal with the suitable wavelength to calculate apparent elastic thickness, we have used the seismogenic layer thickness to characterize the strength of the lithosphere, as already has been done in recent studies (Zhang et al., 2012a,b; Wu and Zhang, 2012). In this context seismogenic layer (hereafter denoted by SL) means the layer wherein the 80% of the seismic energy is released, while any other structure in the crust depicts the non-seismogenic layer (denoted by NSL). In what follows, we briefly present the rheology of the lithosphere in terms of the spatial distribution of the seismicity and the seismic energy released in relation with different transects of TLF.

We compiled data on earthquakes that occurred in the period 1970–2010 as listed in the earthquake catalogue edited by the China Earthquake Network Center, in order to carry out a statistical analysis of the seismic events for each segment of TLF. Besides, we set a lower magnitude limit as $M_L > 1$ to reduce the effect of focal depth errors and uneven monitoring abilities at different places. It should also be noted that the earthquakes occurred in the mouth of 1975.02 have been removed to reduce the aftershock effect from Haicheng earthquake. With reference to the profiles mentioned above (P1 to P4 in Fig. 1), the laterally varying distribution of hypocenters and the statistics of the released energy calculated on a 1° sized grid are presented jointly down to 60 km depth in Fig. 3. The counting of earthquakes was done for those areas closer to the reference profiles (contoured by quadrilaterals in Fig. 1) and the computation following the procedure described by Panza and Raykova (2008) and recently applied by Zhang et al. (2011c,e, 2012a,b). The national seismic network commonly uses the Geiger method (Geiger, 1912) to locate the events, while the provincial seismic networks use the Hypo2000 (Klein and Survey, 2002) and HypoDD (Waldhauser and Ellsworth, 2000) location algorithms. The precision of the seismic event location is commonly scaled as level A (having an uncertainty in focal depth $h \leqslant 5$ km), B ($5 < h \leqslant 15$ km), C ($15 < h \leqslant 30$ km), or D ($h > 30$ km). We herein limit ourselves to seismic events sorted as level A. For each grid cell along any of the profiles, the seismic energy (E) released by an earthquake was computed using its M_S magnitude by means of the relationship $\log E = 11.8 + 1.5\, M_S$ (Panza et al., 2003).

We provide a synoptic representation of the seismogenic properties (spatial distribution of earthquake hypocenters, released seismic energy and number of seismic events) in the uppermost 60 km of the lithosphere at a constant step of 4 km depth intervals. Fig. 3a shows earthquake hypocenters on grid cells at longitude intervals of 1°. Fig. 3b shows the statistics of the logarithm of the seismic energy (log E/Emax) vs. depth as histograms of horizontal filled bars; the maximum value of the energy Emax (used for normalization) is indicated at the bottom of every graph. Fig. 3c shows the distribution of the logarithm of the number of earthquakes vs. depth, and Fig. 3d shows the distribution of log E/min (log E) vs. depth. We can see that both the earthquakes and its energy are unevenly distributed along the four profiles.

Numerous studies have demonstrated that the seismic activity is generally concentrated at different depth ranges. Molnar and Chen (1983) found that the earthquakes that occur on continents are confined in the upper part of the crust, whose brittle nature ensures that earthquakes are relatively common over there. Foster and Jackson (1998) provided evidence that in East Africa, India and Himalayas, earthquakes occur throughout the whole crust, although none below the Moho. In our case, we find a remarkable lateral variation in the thickness of the seismogenic layer. Profiles P1 and P2, that are closer in space, clearly show SL as a layer thicker than in profiles P3 and P4. Compared to other regions, TLF shows a stronger seismic activity inside a relatively thicker seismogenic layer.

In the case of the southernmost segment of TLF (Fig. 3) we find that the seismicity is clearly confined in the upper-to-middle crust (Fig. 3a) and that the seismic energy is mostly released in the upper crust (Fig. 3b). This suggests that the lithospheric strain affects particularly the crust, regardless of whether the uppermost mantle

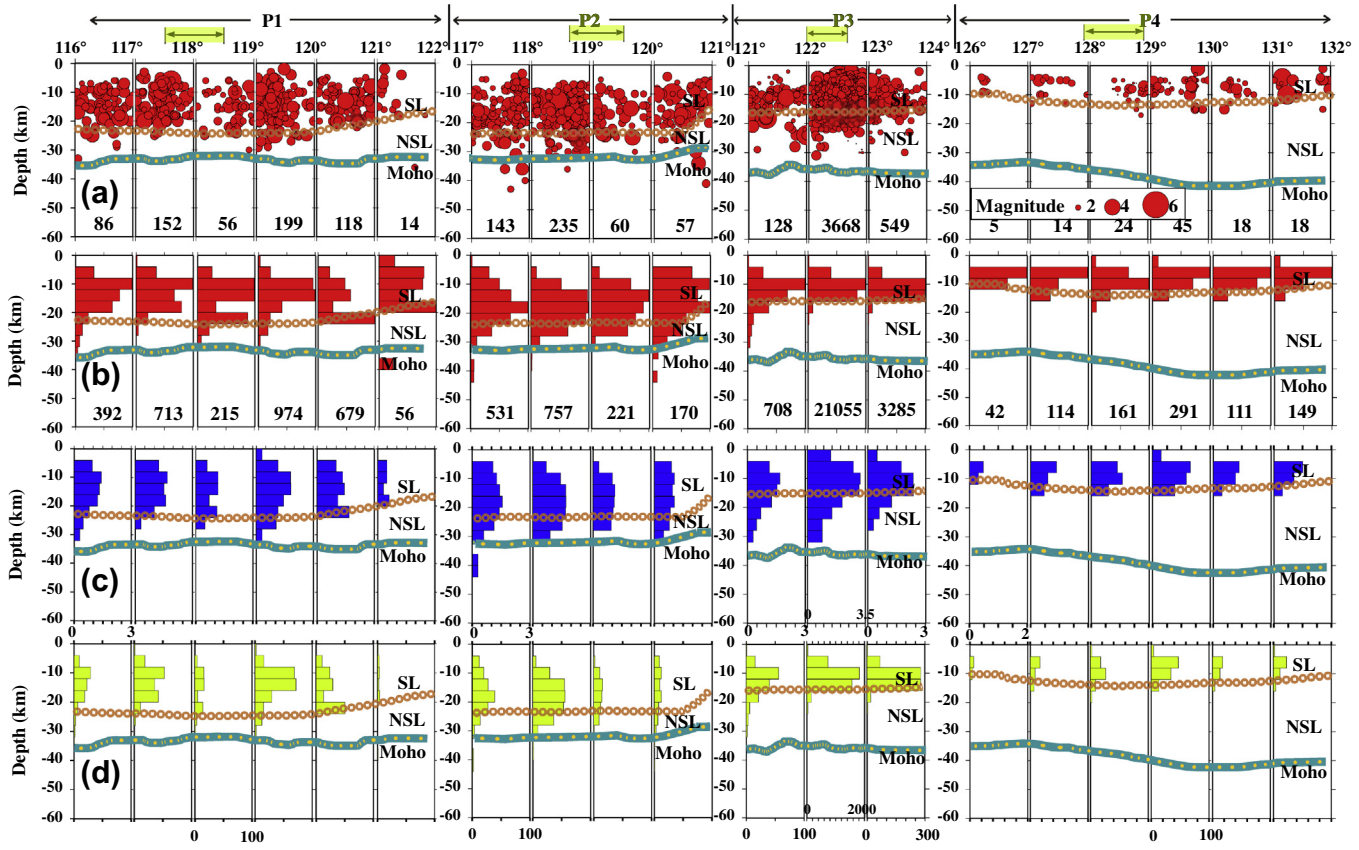

Fig. 3. Earthquakes and seismic energy released inside the quadrilaterals enveloping the profiles P1, P2, P3, and P4 (Fig. 1). Upper panels (a): Earthquake hypocenters (according to magnitude) down to 60 km depth on grid cells at longitude intervals of 1°. The number at the bottom indicates the hypocenters within each longitude interval. As in Fig. 2, the seismogenic (SL) and non-seismogenic (NSL) layers, and the Moho discontinuity have been drawn. Middle panels (b): Statistics of the logarithm of the seismic energy (log E/Emax vs. depth) organized in form of histograms of horizontal filled bars; the maximum value of the energy Emax (used for normalization) is indicated at the bottom of each histogram. Middle panels (c): Distribution of the number of earthquakes, log N vs. depth. Lower panels (d): Distribution of log E/min (log E) vs. depth. The intersection of TLF (East China) with each reference profile is marked on top of the graphs by arrows delimiting a gap in geographic longitude.

may be weak enough to produce some earthquake. The thickness of SL is of about 22 km to the west of TLF, but thins to the east end of the profile. NSL stretches more or less flat in most of the profile with thickness of some 10–12 km, which becomes about 15 km under the east end of the profile (Fig. 3c and d).

On the next segment of TLF, further northward, we observe that the earthquakes occur all over the crust and some of them even below the Moho (Fig. 3a). Nevertheless, the thickness of SL is practically constant of about 24 km along the whole profile except in the east end of the profile where it decreases gradually up to only 12 km (Fig. 3b). NSL shows an underlying flat layer 10-km-thick having similar shape and that rises to the east as SL does (Fig. 3c and d).

On the central segment of TLF (Fig. 3) we find the most active seismicity among the analyzed transects, which is mostly concentrated in the upper crust below the fault belt (Fig. 3a). In particular, the seismic events occur beneath TLF within a much deeper range than in Bohai Bay Basin (west of the profile) and Liaodong Horst (east of the profile), which may be induced by the brittle/ductile transition as observed in the eastern part of the North China Craton (Zhang et al., 2012a). The released seismic energy reaches the maximum value (used for normalization) of 21,000 (Fig. 3b) and the thickness of SL is practically constant of 15–16 km along the whole profile (Fig. 3c). The thickness of NSL is however somewhat greater and fluctuates between 16 and 20 km along the profile (Fig. 3d).

On the northern segment of TLF (Fig. 3), which represents a topographic relief with the highest elevations (Fig. 2d), we find a less frequent and weaker seismic activity (Fig. 3a), and the smallest amount of seismic energy released in the upper crust (Fig. 3b). The GPS results and numerical modeling also show a weak deformation in this part, which mean that the force from West Pacific has been absorbed by the trenches and island arc (Gao et al., 1996; Wang et al., 2002). The thickness of SL varies from 10 to 12 km in the central part of the profile, while NSL shows a bigger thickness from 22 to 24 km along the western half of the profile up to almost 30 km beneath its east end (Fig. 3b–d).

In order to give an overview of the results achieved, we present both the seismic velocity structure and the rheology properties concerning the four investigated profiles (P1 to P4 in Fig. 1) at longitude intervals of 1° in Fig. 4, in terms of thicknesses of the seismogenic and non-seismogenic layers (Fig. 3) and their respective P-wave velocities (Fig. 2), so Fig. 4 allows us to see at a glance all the values of the analyzed variables related to the reference profiles. The intersection of the Tancheng-Lujiang fault belt (East China) with each profile is marked by arrows delimiting a gap in geographic longitude.

5. Geothermal field and temperature distribution

Several researchers have studied the geothermal field providing heat flow measurements along TLF and nearby regions over the past 20 years (Chen, 1988; Zu et al., 1996; Hu et al., 2001; Wang, 2001; Zang et al., 2002; Tao and Shen, 2008). The observed surface heat flow along the reference profiles (P1 to P4 in Fig. 1) varies within a relatively wide range, but not equally in all cases; so, the heat flow is quite similar along the profiles P1 and P2 and shows an increase from west to east from 58 to about 67 mW/m^2 and from 59 to 66 mW/m^2 (Fig. 5a and b, upper panels). However, a negative gradient is observed in the other two profiles, decreasing very rapidly from 66 to 57 mW/m^2 in the case of P3 and somewhat smoother from 68 to 63 mW/m^2 in the case of P4 (Fig. 5c and d, upper panels).

The temperature field was calculated along the reference profiles down to a depth of 55 km, using of a two-dimensional numerical solution of the steady-state heat conduction equation, obtained after modeling the medium by finite elements (Hu et al., 2001). This solution was constrained by surface and basal heat flows, temperature-dependent thermal conductivity (Cermak and Bodri, 1986) and heat production (Rybach and Buntebarth, 1984; Cermak and Rybach, 1989) in the continental crust. The procedure here followed is similar to the method applied by Zhang et al. (2008). The uncertainties affecting the temperature field are estimated to be about 15% according to those associated to the surface heat flow measurements (Pasquale et al., 1990).

The Moho temperature is found between 500 and 650 °C in the profiles P1, P2 and P3 (Fig. 5a–c, lower panels), but increases slightly up to values of 650–700 °C along the profile P4 (Fig. 5d, lower panel). In the upper-to-middle crust, the temperature field correlates with the smooth regional variation of the surface heat flow (CEA, 1992; Jin et al., 1996), whereas the temperature fluctuation in the lower crust and topmost mantle are constrained by the heat flow changes in these layers (Zhang et al., 2008, 2011d).

6. Discussion

6.1. Segmentation properties of TLF

A synthesis of data from seismic velocity structure of the crust (Fig. 2), seismic activity and crustal rheology (Fig. 3), average P-wave velocity in SL and NSL (Fig. 4), and surface heat flow and temperature field (Fig. 5), provides us robust information to discuss the Tancheng-Lujiang fault belt and it physical segmentation. To facilitate understanding of the geophysical responses derived from the segmentation of TLF, we have integrated all the available geophysical information together with the topographic relief along the fault (top panel) and penetration depth (bottom panel) from 31°N to 46°N in Fig. 6. As can be seen, the topographic relief is rather flat, except in the north transect of the fault where the higher elevations make its appearance. The highest concentration of earthquakes in the crust occurs between 35° and 39°N approximately, though other earthquakes also occur at deeper depths below the Moho. SL is clearly thicker at latitudes of ~35–39°N and ~43.5–45°N. The Moho is a slightly undulated interface that hardly shows any variation around 30–34 km depth, but rises a little at the central part of the fault belt (36–40°N) where the crust is about 2 km thinner than elsewhere. The heat flow is around 65 mW/m^2, remains stable up to 37.4°N and increases slightly with smooth ups and downs from this latitude to the north end of the fault. Fig. 6, which provides an overview of TLF at different latitudes, shows distinctive zoning features that refer to the following aspects: (1) seismogenic layer thickness; (2) crustal thickness; (3) crustal P-wave velocity; (4) heat flow; and (5) penetration depth. Below we summarize these zoning features for different fault segments (S1 to S3 in Fig. 6a).

6.1.1. Segment S1 (latitude 31–34.5°N)

This segment (Fig. 6a) is characterized by a gradually thickening of SL northward together with a thinning of NSL in this direction, with earthquakes mostly confined in the upper crust (Fig. 6b and c). The crustal thickness is about 34 km (Fig. 6c). The crust-mantle layered seismic velocity structure just below the middle point A (Fig. 6a) is represented by the 1D crustal velocity column marked by A (Fig. 6d). An important feature is that P-wave velocity increases from 6.8 to 7.1 km/s within the lower crust 10-km-thick, which suggests there is a mafic layer at the bottom of the crust. The high heat flow is distributed all over the Tanlu fault and stays almost stable at 65 mW/m^2 (Fig. 6e). According to the depth of formation of peridotite xenoliths (Wan et al., 1996), the penetration of the fault reaches 80 km but then rises up to 60 km from south to

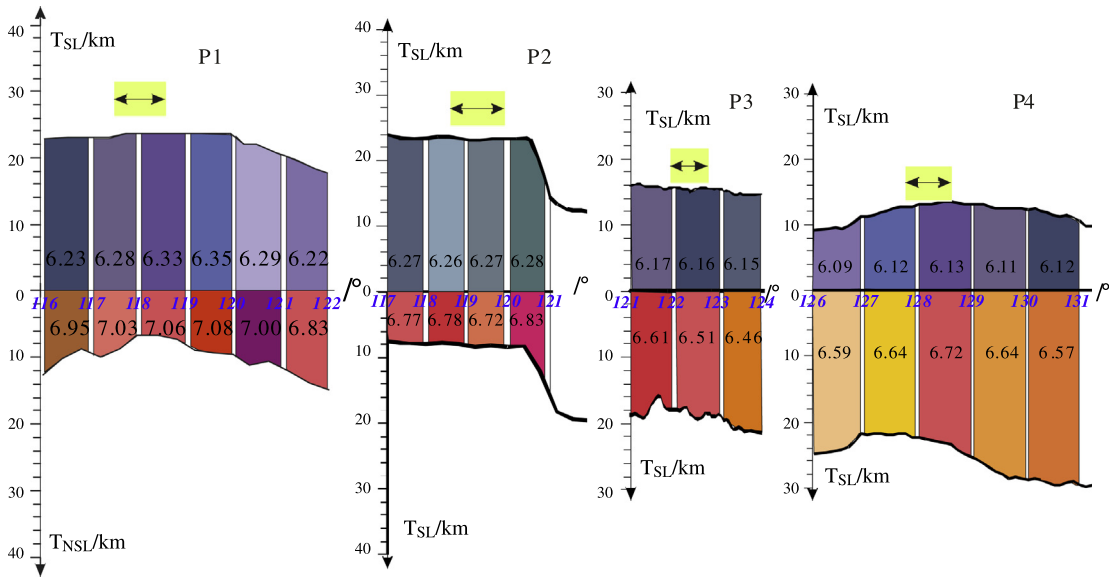

Fig. 4. Average P-wave velocity (in km/s) and thickness of the seismogenic (T_{SL}) and non-seismogenic (T_{NSL}) layers at longitude intervals of 1° regarding the reference profiles analyzed in this study (P1 to P4 in Fig. 1). The intersection of TLF (East China) with each reference profile is marked on top of the graphs by arrows delimiting a gap in geographic longitude.

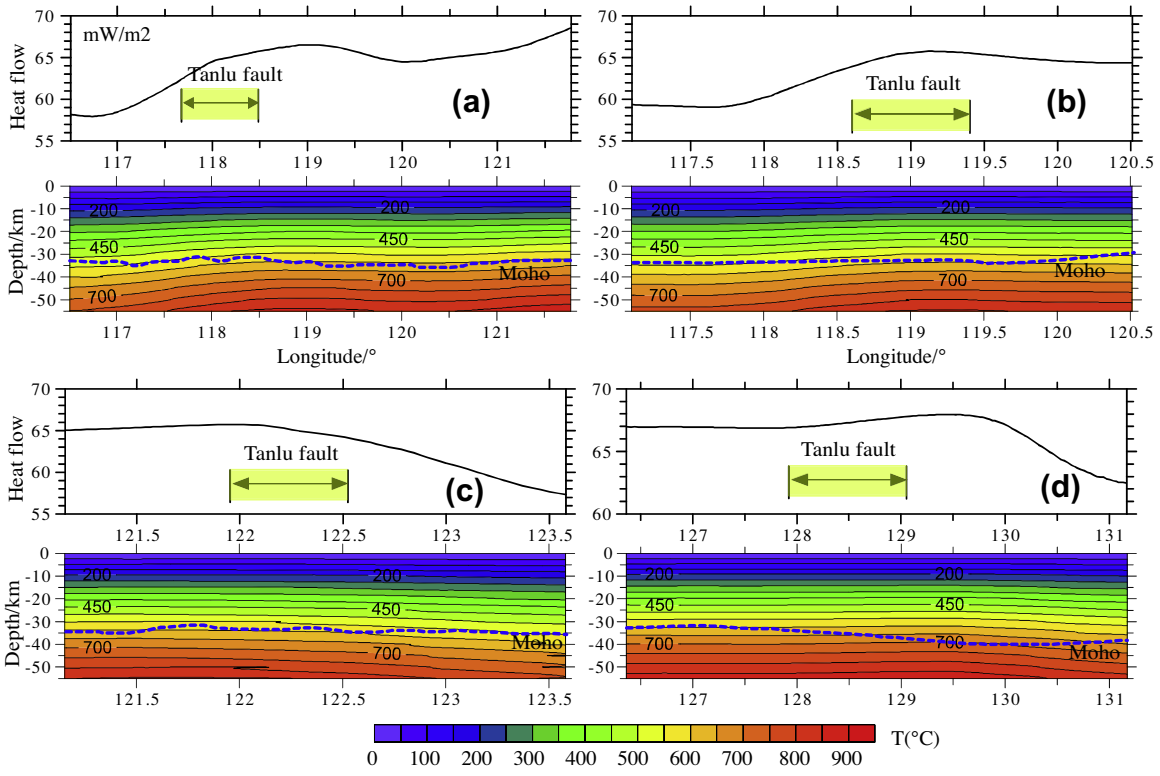

Fig. 5. Surface heat flow (top panels a, b, c and d) and temperature distribution in the crust and uppermost mantle (bottom panels) related to the four reference profiles (P1 to P4 in Fig. 1). The intersection of TLF (East China) with each reference profile is marked by arrows delimiting a gap in geographic longitude.

north (Fig. 6f), which is consistent with the depth estimated from a magnetotelluric sounding (Zhu et al., 2002).

6.1.2. Segment S2 (latitude 34.5–42°N)

The thickest SL and the thinnest NSL characterize this segment at its southern half (Fig. 6a). In this sector SL is deeper than 25 km and thicker than NSL, which is only about 5 km thick. The seismic activity is remarkable in this zone with many earthquakes occurred at different crustal depths and even at mantle depths, and likewise the seismic energy that is released in the crust (Fig. 6b and c). The Moho depth is 30–32 km (Fig. 6c). Analogously, the 1D crustal velocity column marked by B (Fig. 6d) represents now the crust-mantle seismic velocity structure in this sector just below the point B at surface (Fig. 6a). Like in the previous case, the P-wave velocity increases from 6.7 to 7.4 km/s within the lower crust 10-km-thick, which suggests the presence of a mafic layer

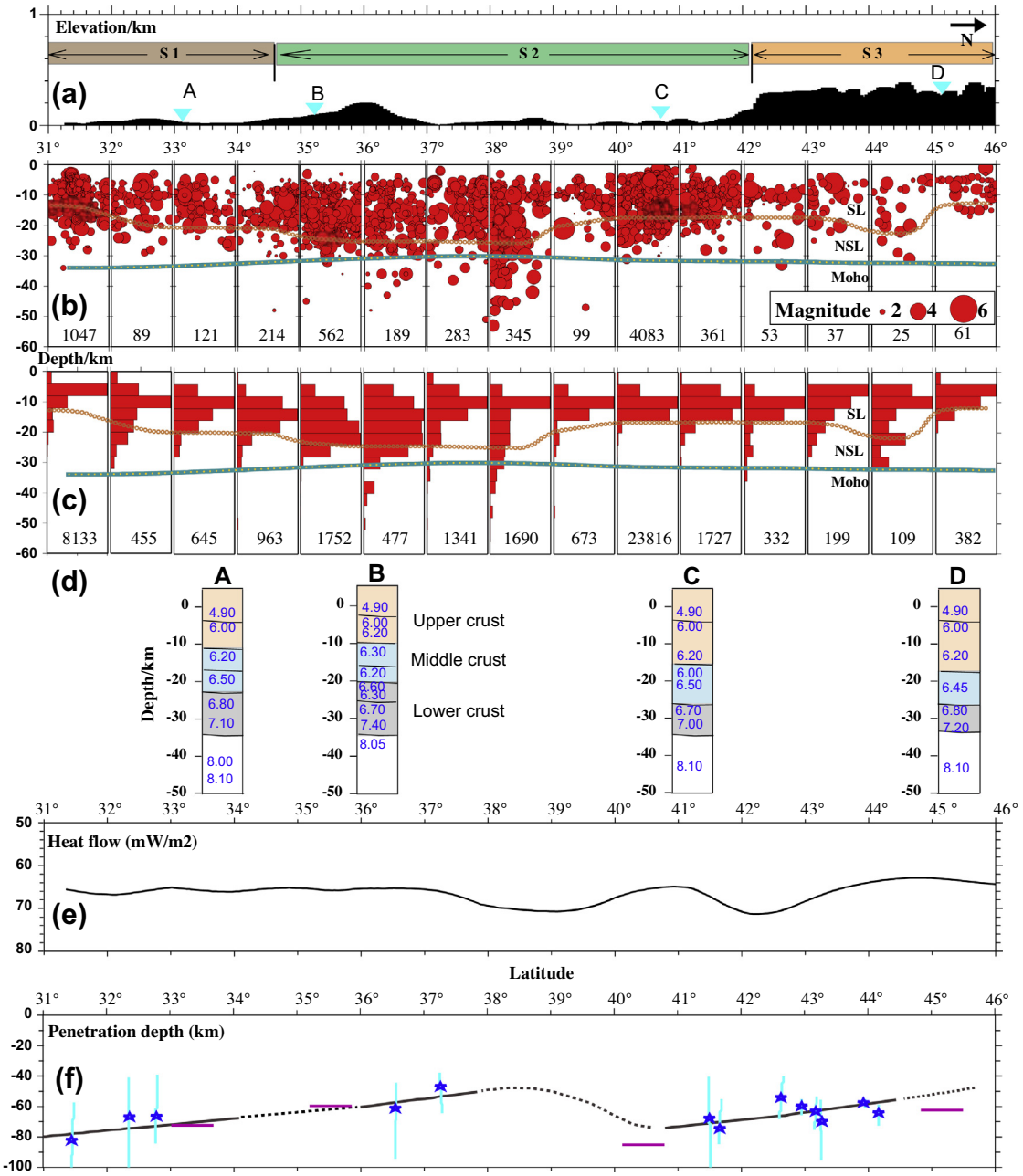

Fig. 6. Geophysical features along TLF between 31°N and 46°N at latitude intervals of 1°. Panel (a): Topographic relief (data based on GTOPO30) along the segments S1 (Anhui and Jiangsu provinces), S2 (south of Shandong province to Shenyang, Liaoning province) and S3 (Jilin and Heilongjiang provinces). Panel (b): Earthquake hypocenters (according to magnitude) down to 60 km depth on grid cells at latitude intervals of 1°. The number at the bottom indicates the hypocenters within each latitude interval. The seismogenic (SL) and non-seismogenic (NSL) layers, and the Moho discontinuity have been drawn. Panel (c): Statistics of the logarithm of the seismic energy (log *E*/Emax vs. depth) organized in form of histograms of horizontal filled bars; the maximum value of the energy Emax (used for normalization) is indicated at the bottom of each latitude interval. Panel (d): P-wave velocity (in km/s) vertically distributed under the positions marked by A, B, C and D at surface. Panel (e): Heat flow along TLF (after Tao and Shen, 2008). Panel (f): Penetration depth estimated from the formation depth of peridotite xenoliths (Wan et al., 1996); the stars indicate depths of peridotite xenoliths and the error bars reflect possible depth ranges; black lines depict average depths calculated from the stars, while dot lines depict depths extrapolated from the black lines in the most reasonable way; finally, the other lines mark the penetration depth given by a magnetotelluric sounding.

(with a strong vertical velocity gradient) at the bottom of the crust. In the northern half of S2 (Fig. 6a) SL is a comparatively thinner layer with earthquakes mostly confined in the upper crust, although the seismic activity is strong in this part since the released energy reaches the value of 23,000 (Fig. 6b and c). The crustal thickness is 33 km here (Fig. 6c) and the 1D crustal velocity column marked by C (Fig. 6d) describes the seismic velocity structure in this zone. The heat flow rises and is somewhat higher than in the first sector up to 70 mW/m^2 (Fig. 6e), thus suggesting underplating or crust/mantle interaction (Zhang et al., 2012a). Based on the formation depth of the peridotite xenoliths (Wan et al., 1996), the fault penetrates in this sector to 50–55 km, although further north it reaches the deepest point at 75 km beneath the seismic zone of Haicheng (Fig. 6f), which is roughly consistent with the depth estimated from a magnetotelluric sounding (Zhu et al., 2002). The heat flow seems to show a mirror symmetry with the penetration depth of the fault even though it has been extrapolated (Fig. 6e and f). The rock fragmentation inside the lithosphere can result in many earthquakes and high heat flow in segment S2. This is the causative mechanism for the seismicity in this area. Both

phenomena may be coincident because the fragmentation of rocks is the triggering factor of earthquakes, and the faults can be the passage for heat flow.

6.1.3. Segment S3 (42–46°N)

The northernmost transect (Fig. 6a) is characterized by a thick SL down to 20 km depth and a rather weak seismic activity (Fig. 6b and c). The Moho depth is 32–33 km (Fig. 6c). The crust-mantle seismic velocity structure in this sector is given by the 1D crustal velocity column marked by D (Fig. 6d). Here the P-wave velocity also increases from 6.8 to 7.2 km/s within the lower crust 10-km-thick, which again suggests there is a mafic layer at the bottom of the crust. The heat flow is relatively high ~66 mW/m^2 along this segment S3 (Fig. 6e). Here the fault penetrates between 50 and 60 km and already reaches the uppermost mantle (Fig. 6f) as revealed by the formation depth of the peridotite xenoliths (Wan et al., 1996), which agrees partly with the depth estimated by a magnetotelluric sounding (Zhu et al., 2002), the latter yielding somewhat greater depths (Fig. 6f). The low seismicity in the Songliao basin, the northernmost transect of TFL, may be because of the thrust force developed by the West Pacific in the area is absorbed by the trenches and island arc. In fact, GPS results (Wang et al., 2002; Ge and Zhang, 2009) and the results from by numerical modeling (Gao et al., 1996) show a weak deformation in the basin.

6.2. Segmentation mechanism of TLF

The formation mechanism of TLF in East China has been debated ever since its finding through aeromagnetic measurements in the 50s and the mapping of the surface geology and tectonics in the 60s (Xu, 1984a,b). So far, four tectonic models have been proposed to explain the formation of TLF: (1) A slip fault system as consequence of the collision between the Yangtze Block and the North China Block (Cluzel et al., 1991; Yin and Nie, 1993); (2) A strike-slip fault system accommodated to the oblique convergence between the Pacific oceanic plate and the Asian continent (Xu et al., 1987, 1993; Zhu et al., 2004, 2012); (3) A transform fault in the margin between North China and South China due to the dynamics of the Pacific oceanic plate (He et al., 1990; Wang and Cheng, 1992); (4) A transform fault generated through the collision between South China and North China along the Qinling-Dabie orogeny (Zhang et al., 1984; Guo, 1993). Essentially, these tectonic models can be evaluated by combining the various models into the interaction between the North and South China Blocks (2,3) or that between the Pacific plate and North China (1,4).

In the first interaction model, the lower crust beneath the segment S1 and the southernmost part of the segment S2 should be that of the Yangtze Block, or else it should be the same or similar that beneath the NCC. In the course of the back-arc extensional activity during the Late Cretaceous to the Eogene (Yin, 2010), an intense upwelling of the asthenosphere occurred under the fault zone in North China, which resulted in a lithospheric narrowing of pure shear type (Zhu et al., 2004; Yang et al., 2012) and the probable rock fragmentation inside the lithosphere. As a consequence of this upwelling along the fracture zone, both the temperature and the geothermal flow in the north transect of S2 should be higher than elsewhere and the broken rocks should generate more earthquakes. The Dabie–Sulu orogenic belt, adjacent to the south part of TLF, resulted from the continental collision between the Yangtze Block and the NCC since Mesozoic accompanied by ultra-high pressure metamorphism (Zhu and Zheng, 2009; Bai et al., 2007), so the crustal P-wave velocity in S1 should be higher. In order to evaluate this possibility, we have chosen a crustal P-wave velocity column obtained in South China (Zhang et al., 2005) and another in North China (Zhang et al., 2011d) with the purpose of comparing with other two velocity columns beneath

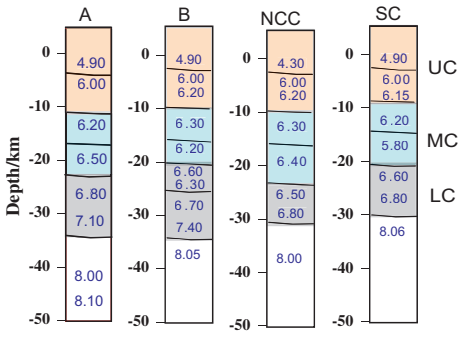

Fig. 7. P-wave velocity (in km/s) shown in columns below the positions A and B (the same as in Fig. 6), North China Craton (NCC) and South China (SC) (these two last indicated by triangles in Fig. 1). UC: Upper crust; MC: Middle crust; LC: Lower crust.

the segments S1 and S2 (points A and B at surface, Fig. 6). All these columns are shown together in Fig. 7. We can observe that the similarity of the velocity-depth profiles for South China and the segment S1 is much higher, which supports the idea that the formation of S1 has a close relationship with the collision between the Yangtze and North China Blocks (Yin and Nie, 1993). In addition, the segment S1 shows a seismic layer 15 km thick similar to that of the Yangtze Block (Zhang et al., 2012b).

As to the wrench model, which proposes that TLF is a rift formation subjected to the continuous convergence of the Pacific plate onto the Asian plate, geophysical experiments in the rifts or wrenches around the world demonstrate that a high P-wave velocity layer usually exists at the bottom of the crust, which suggests that underplating is a key mechanism to trigger rifting or wrench. This P-velocity reaches 7.2 km/s in the lower crust beneath the Kenya Rift (Thybo et al., 2000), 7.3–7.5 km/s in central Denmark (Thybo et al., 2006), >7.4 km/s in the Baikal Lake area (Thybo and Nielsen, 2009), and 7.2 km/s in the Three Gorges area of the Yangtze Platform, central China (Zhang et al., 2009). In view of the 1D crustal velocity columns beneath the above mentioned segments of TLF (Fig. 7), we see layers with velocities as high as 7.1 km/s or even 7.4 km/s beneath the segment S1 and the southern transect of the segment S2, respectively, but no layer with P-velocity beyond 7.0 km/s beneath the northern part of the segment S2. Li (1994) proposed a crustal-detachment model of suture for the region east of TLF, which suggests that the upper crust of the South China Block in the Subei-Yellow Sea region was detached from the lower crust and thrust over the North China block for >400 km, whereas the lower part of the lithosphere was subducted under the North China Block along a subsurface suture running to east from Nanjing. The sinistral offset of the Qinling suture by TLF is only 110–120 km in the deep crust and much less than previously suggested. In this way the layer with P-velocity > 7.0 km/s could not have been induced by underplating (Thybo et al., 2000, 2006; Zhang et al., 2011d, 2012a), but acts as a signature of the subduction of the lower part of the lithosphere under South China where the seismic velocity would increase as the pressure (depth) increases (Wang et al., 2000).

6.3. TLF-lithosphere interaction in East China

The lithosphere beneath TLF and part of the North China Craton is heterogeneous both in mineralogy and chemistry (Wu et al., 2003, 2005; Zhang et al., 2011b). The incidence of TLF upon the evolution of East China is one of the most interesting topics in this context, which can be evaluated from geophysical and geochemical observations. Besides the high heat flow and strong seismicity mentioned in the previous section, receiver functions show an

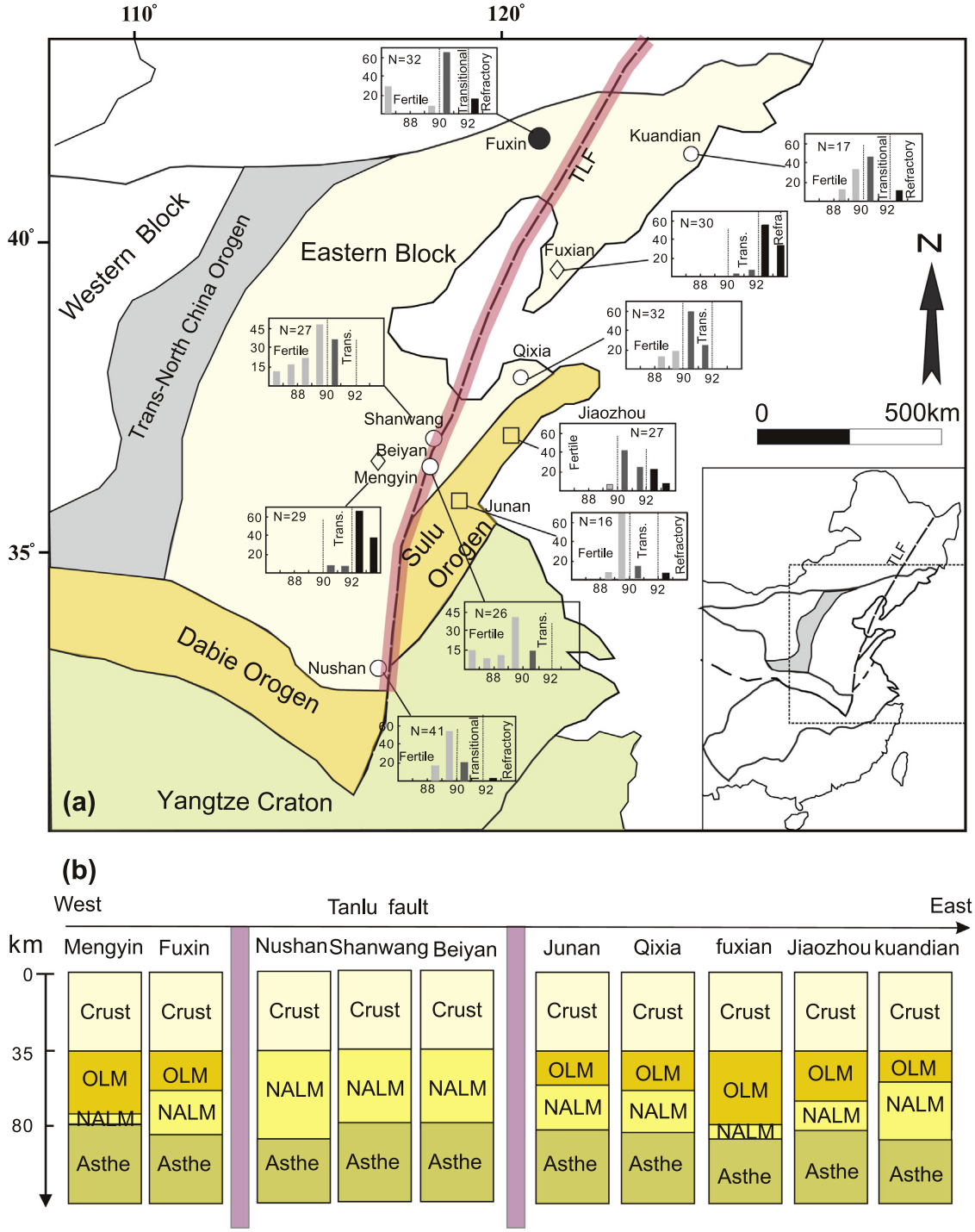

Fig. 8. (a) Distribution of olivine-Mg# in peridotites, East China: Fertile, olivine-Mg# < 90; Transitional (Trans), olivine-Mg# 90–92; Refractory (Refra), olivine-Mg# > 92. Data sources: Leiyan (Xiao et al., 2010); Jiaozhou (Zhang et al., 2011a); more details can be seen in Zheng et al. (2007b). The involved region is outlined by a rectangle drawn on a situation map of East China (bottom right corner). (b) The lithospheric architecture around TLF, East China: OLM means Old Lithospheric Mantle; NALM means Newly Accreted Lithospheric Mantle; Asthe is the abbreviation for Asthenosphere.

uplift of the Moho and thickening of the lithosphere under TLF (Chen et al., 2006; Zheng et al., 2006, 2007a), which seems to indicate that the Tanlu fault zone might have acted as a major channel for the upwelling of the asthenosphere during the Mesozoic–Cenozoic continental extension and lithospheric thinning in eastern China. In addition, the results obtained from P-wave and S-wave velocity tomography show low velocity anomalies below TLF, which may also reflect asthenospheric upwelling in this region (Tian et al., 2009; Tian and Zhao, 2011).

According to recent petrologic and geochemical studies in NCC (Zheng et al., 2001, 2007b, 2008; Wu et al., 2003, 2005, 2006; Zhang et al., 2003b, 2010a; Ying et al., 2006; Xiao et al., 2010; Xu et al., 2012; Zhang et al., 2011b; Zhang, 2012), the low-Mg# lherzolites have petrologic and mineralogical affinities with mantle peridotitic xenoliths from the Cenozoic basalts of NCC and represent the newly accreted lithospheric mantle. In contrast, the high-Mg# lherzolites have petrologic features similar to mantle peridotitic xenoliths from the Archean/Proterozoic lithospheric

mantle and represent the remnant old refractory lithospheric mantle. However, the percentages of high-Mg# and low-Mg# peridotites vary (Zheng et al., 2007b; Xiao et al., 2010; Zhang et al., 2011b) (Fig. 8a).

The majority of the xenoliths from Qingdao are high-Mg#, with small amounts of low-Mg# peridotites and Archean lower crust granulites (Zhang and Zhang, 2007), while the xenoliths from Junan are mainly low-Mg# peridotites, with only one high-Mg# peridotite reported so far, although there are abundant lower crustal granulite xenoliths (Xiao et al., 2010). Fertile peridotites are rare in the xenolith suites from the Paleozoic Mengyin and Fuxian kimberlites (Zheng et al., 2007b). In the xenolith suites from Mesozoic–Tertiary basalts, the proportion of fertile peridotites is clearly higher in some localities near the trans-lithospheric TLF zone, while more refractory components are commonly preserved in more distant localities such as Hebi, Fuxin and Kuandian (Zheng et al., 2007b). The lithospheric mantle beneath the Qingdao region is composed of a small amount of newly accreted material and dominant ancient lithospheric mantle component that was substantially modified. The Junan, Kuandian and Fuxin lithospheric mantles are mainly composed of newly accreted lithospheric mantle, with only a small amount of residual ancient mantle at the top upper mantle. All the peridotitic xenoliths entrained in the Late Mesozoic basaltic rocks in Qingdao, Daxizhuang and Junan, eastern Shandong, are spinel-facies, and no garnet-facies xenoliths have been found, suggesting that the thickness of the lithosphere is less than 75–80 km (Xiao et al., 2010). This inference is consistent with the result of the geophysical exploration of TLF and its neighboring regions (Chen et al., 2006). The Beiyan basalts located within TLF and their entrained peridotites are very low in olivine Fo values, among which the highest Fo value is close to that of Junan low-Mg# peridotites. This suggests that the lithospheric mantle beneath the TLF zone is composed of newly accreted mantle, without remnants of old lithospheric mantle, unlike what happens in the surrounding zones (Fig. 8b).

Abundant cpx-rich lherzolites and wehrlites with extremely low Fo (<87) values and high $^{187}Os/^{188}Os$ ratios also occur in the interior of the TLF zone beside the Beiyan locality, such as Nushan in Anhui Province (Xu et al., 1998; Xiao and Zhang, 2011) and Shanwang in Shangdong Province (Zheng et al., 1998; Xiao and Zhang, 2011). Therefore, the TLF zone facilitates the ascent of the asthenosphere and enhances the degree of peridotite-melt reaction (Wu et al., 2006; Zhang, 2009; Xiao and Zhang, 2011; Zeng et al., 2011).

7. Concluding remarks

The segmentation properties of TLF along its stretch between 31°N and 46°N of latitude is identified based on a synthesis of the results obtained from integrated geophysical data set along four vertical sections that cut the fault in NW–SE direction at latitudes of 31–34°N, 34.3–35.8°N, 39.9–41.2°N and 44.5–45.4°N approximately. These results specifically relate to crustal seismic velocities, Moho depth, earthquake hypocenters, seismic energy released, seismogenic layer and crustal rheology, heat flow and geothermal field, and penetration depth of the fault. The north-to-south segmentation of TLF can be summarized in the following terms: (1) south segment: the highest seismic velocities comparatively, the crust is relatively thicker, seismicity constrained in the upper-to-middle crust, penetration depth of the fault 60–80 km; (2) middle segment: earthquakes occur at deeper depth even below the Moho, the most intense seismic activity and the bigger amount of released energy, the deepest seismogenic layer, the penetration depth undulates between 50–75 km, and the heat flow shows positive correlation with the penetration depth; (3) north segment: a contrasting picture with the highest topographic relief, a less frequent and weaker seismic activity wholly concentrated in the shallowest crustal layers, low amount of seismic energy released in the upper crust, and relatively high Moho temperature, and penetration depth of the fault 50–65 km.

The formation of the south transect of TLF is closely related to the collision between the Yangtze Block and the North China Block, as supported by the higher crustal P-wave velocity observed. However the layer with P-velocity > 7.0 km/s could not have been induced by underplating, but acts as signature of the subduction of the lower part of the lithosphere of South China.

From the geophysical and geochemical data, TLF plays an important role in the evolution of the lithospheric mantle beneath East Asia, acting as a deep channel for the ascent of melts and fluids, resulting in higher heat flow, higher seismicity, lower P-wave velocity anomaly, thinner lithosphere, higher degree of lithospheric modification and a greater amount of newly accreted lithosphere near the fault.

Acknowledgements

We are very grateful to all those people and institutions that provided data and interpretations from geophysical experiments related to the study area. We thank Jianping Zheng who kindly gave us the material for Fig. 8. Thanks also to Guang Zhu, Jing Wu, Xi Zhang and Lin Chen for making fruitful discussions with us. We also thank the Editor-in-Chief Bor-ming Jahn, the editor M. Santosh, Irene Yao and three anonymous reviewers for their constructive comments and suggestions, which significantly improved the manuscript. This research benefited from the financial support granted by the Ministry of Land and Resources (Sinoprobe-02-02) and the National Nature Science Foundation of China (41021063).

References

Audet, P., Jellinek, A.M., Uno, H., 2007. Mechanical controls on the deformation of continents at convergent margins. Earth and Planetary Science Letters 264 (1–2), 151–166.

Bai, Z.M., Zhang, Z.J., Wang, Y.H., 2007. Crustal structure across the Dabie–Sulu orogenic belt revealed by seismic velocity profiles. Journal of Geophysics and Engineering 4, 436–442.

Burov, E.B., 2010. The equivalent elastic thickness, seismicity and the long-term rheology of continental lithosphere: time to burn-out "crème brûlée"? Insights from large-scale geodynamic modeling. Tectonophysics 484 (1), 4–26.

Burov, E.B., Watts, A.B., 2006. The long-term strength of continental lithosphere: jelly sandwich or crème brûlée? GSA Today 16, 4–10.

CEA, 1992. Geoscience Transect from Dong Ujimqinqi, Nei Mongol, to Donggou, Liao, China. Seismological Press, Beijing, 1992.

Cermak, V., Bodri, L., 1986. Two-dimensional temperature modelling along five East-European geotraverses. Journal of Geodynamics 5, 133–163.

Cermak, V., Rybach, L., 1989. Vertical distribution of heat production in the continental crust. Tectonophysics 159, 217–230.

Chen, M.X., 1988. Geothermics of North China. Science Press, Beijing, pp. 218.

Chen, L., 2010. Concordant structural variations from the surface to the base of the upper mantle in the North China Craton and its tectonic implications. Lithos 120, 96–115.

Chen, H., Zhang, Y., Xu, S., 1999. The Lithospheric Textural and Structural Features as well as Oil and Gas Evaluation in the Lower Yangtze Area and its Adjacent Region. Geological Publishing House, Beijing (in Chinese).

Chen, H.Y., Shu, L.S., Zhang, Y.Y., Lin, C.M., Liu, G.H., Zhao, Y.Y., 2004. Mesozoic–Cenozoic tectonic evolution of the Hefei Basin. Geological Journal of China Universities 10 (2), 250–256 (in Chinese with English abstract).

Chen, L., Zheng, T.Y., Xu, W.W., 2006. A thinned lithospheric image of the Tanlu Fault Zone, eastern China: constructed from wave equation based on receiver function migration. Journal of Geophysical Research 111 (B9), B09312.

Cluzel, D., Lee, B.J., Cadet, J.P., 1991. Indosinian dextral ductile fault system and synkinematic plutonism in the southwest of the Ogcheon belt (South Korea). Tectonophysics 194 (1–2), 131–151.

Deng, Y.F., Li, S.L., Fan, W.M., Liu, J., 2011. Crustal structure beneath South China revealed by deep seismic soundings and its dynamics implications. Chinese Journal of Geophysics 54 (10), 2560–2574. http://dx.doi.org/10.3969/j.issn.0001-5733.2011.10.013 (in Chinese with English abstract).

Dou, L.R., Song, J.G., Wang, Y., 1996. Chronology of the formation of the northern Tan-lu fault zone and its implications. Geological Review 42 (6), 508–512 (in Chinese with English abstract).
Fan, W.M., Menzies, M.A., 1992. Destruction of aged lower lithosphere and accretion of asthenosphere mantle beneath eastern China. Geotectonica et Metallogenia 16 (2), 171–180.
Fan, W.M., Zhang, H.F., Baker, J., Jarvis, K.E., Mason, P.R.D., Menzies, M.A., 2000. On and off the North China Craton: where is the Archaean keel? Journal of Petrology 41, 933–950.
Fan, W.M., Guo, F., Wang, Y.J., Zhang, H.F., 2007. Late Mesozoic magmatism from the North China Block: constraints on chemical and isotopic heterogeneity of the subcontinental lithospheric mantle. In: Zhai, M.G., Windley, B.F., Kusky, T.M., Meng, Q.R. (Eds.), Mesozoic Sub-Continental Lithospheric Thinning Under Eastern Asia, vol. 280. Geological Society of London Specical Publicaton, pp. 77–100.
Foster, A.N., Jackson, J.A., 1998. Source parameters of large African earthquakes, implications for crustal rheology and regional kinematics. Geophysical Journal International 134 (2), 422–448.
Fu, W.Z., Yang, B.J., 1998. Study on the seismology in Manzhouli–Suifenhe geoscience transect of China. Journal of Changchun University of Science and Technology 28, 206–212 (in Chinese with English abstract).
Gao, X.L., Luo, H.Y., Hirahara, K., 1996. Numerical model of stress generation and transfer caused by the Japanese subduction zone. Seismology and Geology 16 (2), 97–108 (in Chinese with English abstract).
Ge, R.F., Zhang, Q.L., 2009. Seismic activity and stress state of the northern Tanlu Fault zone and its adjacent areas. Seismology and Geology 31 (1), 141–154 (in Chinese with English abstract).
Geiger, L., 1912. Probability method for the determination of earthquake epicenters from the arrival time only. Bulletin of St. Louis University 8 (1), 56–71.
Guo, Z.Y., 1993. Structure, mechanism and history of the middle segment (Yishu Belt) of the Tancheng-Lujiang fault zone. In: Xu, J.W. (Ed.), The Tancheng-Lujiang Wrench Fault System. John Wiley and Sons Ltd., pp. 77–88.
He, Y.M., Jia, D., Shi, Y.S., 1990. The new understanding of the Tanlu fault – from the terrane collage to see the Tanlu fault evolution. Journal of Nanjing University (Natural Sciences) 4, 85–93 (in Chinese with English abstract).
Hou, M.J., Wang, Y.M., Jacques, M., Pierre, V., 2003. Dynamic evolution and tectonic significance of the Tanlu fault zone (Anhui segment). Geological Bulletin of China 22 (2), 105–112 (in Chinese with English abstract).
Hsiao, L.Y., Graham, S.A., Tilander, N., 2004. Seismic reflection imaging of a major strike-slip fault zone in a rift system: Paleogene structure and evolution of the Tan-Lu fault system, Liaodong Bay, Bohai, offshore China. AAPG Bulletin 88 (1), 71–97.
Hu, S.B., Wang, J.Y., He, L.J., 2001. Compilation of heat flow data in the China continental area (third edition). Chinese Journal of Geophysics 44 (5), 610–626 (in Chinese with English abstract).
Huang, J.L., Zhao, D.P., 2006. High-resolution mantle tomography of China and surrounding regions. Journal of Geophysical Research 111 (B9), B09305. http://dx.doi.org/10.1029/2005JB004066.
Jin, X., Ehara, Xu, H.P., 1996. Thermal structure and heat flow geotraverse along Manzhouli–Suifenhe, China. Chinese Science Bulletin 40 (2), 161–163 (in Chinese with English abstract).
Klein, F.W., Survey, G., 2002. User's guide to HYPOINVERSE-2000: a Fortran program to solve for earthquake locations and magnitudes. US Geological Survey 14–27.
Li, T.S., 1991. Features of gravity and magnetic anomalies and crust structure along the Lianyungang–Linyi–Sishui profile. Journal of Seismological Research 14 (2), 141–146 (in Chinese with English abstract).
Li, Z.X., 1994. Collision between the North and South China blocks: a crustal-detachment model for suturing in the region east of the Tanlu fault. Geology 22 (8), 739–742.
Li, J.L., Chao, H.T., Cui, Z.W., Zhao, Q.Y., 1994. Segmentation of active fault along the Tancheng-Lujiang fault zone and evaluation of strong earthquake risk. Seismology and Geology 16 (2), 121–126 (in Chinese with English abstract).
Li, S.L., Mooney, W., Fan, J., 2006a. Crustal structure of mainland China from deep seismic sounding data. Tectonophysics 420 (1–2), 239–252.
Li, Y.P., Wu, S.G., Han, W.G., Zhang, Y.Q., 2006b. A study on geophysical features of deep structures of the Hefei Basin and the southern Tan-Lu fault zone. Chinese Journal of Geophysics 49 (1), 115–122 (in Chinese with English abstract).
Li, S., Zhao, G., Dai, L., Liu, X., Zhou, L., Santosh, M., Suo, Y., 2012a. Mesozoic basins in eastern China and their bearing on the deconstruction of the North China Craton. Journal of Asian Earth Sciences 47, 64–79.
Li, S.Q., Chen, F., Siebel, W., Wu, J.D., Zhu, X.Y., Shan, X.L., Sun, X.M., 2012b. Late Mesozoic tectonic evolution of the Songliao basin, NE China: evidence from detrital zircon ages and Sr–Nd isotopes. Gondwana Research 22, 943–955.
Liang, C., Song, X., Huang, J., 2004. Tomographic inversion of Pn travel times in China. Journal of Geophysical Research 109, B11304. http://dx.doi.org/10.1029/2003JB002789.
Lu, Z.X., Xin, H.K., 1993. Geoscience transect from Dong Ujmqinqi, Nei Mongol, to Donggou, Liaoning, China. Chinese Journal of Geophysics 36 (6), 765–772 (in Chinese with English abstract).
Ma, X.Y., 1989. Lithospheric Dynamics Atlas of China. China Cartographic Publishing House, Beijing (in Chinese).
Ma, X.Y., Wu, D.N., 1987. Cenozoic extensional tectonics in China. Tectonophysics 133, 243–255.
Ma, X.Y., Liu, C.Q., Liu, G.D., 1991. Xiangshui (Jiangsu Province) to Mandal (Nei Mongol) Geoscience Transect. Acta Geologica Sinica 3, 199–215 (in Chinese with English abstract).
Maggi, A., Jackson, J., McKenzie, D., Priestley, K., 2000. Earthquake focal depths, effective elastic thickness, and the strength of the continental lithosphere. Geology 28, 495–498.
Martin, M., Xu, Y.G., Zhang, H.F., Fan, W.M., 2007. Integration of geology, geophysics and geochemistry: a key to understanding the North China Craton. Lithos 96, 1–21.
Molnar, P., Chen, W.P., 1983. Focal depths and fault plane solutions of earthquakes under the Tibetan plateau. Journal of Geophysical Research 88 (B2), 1180–1196.
Mount, V.S., Suppe, J., 1987. State of stress near the San Andreas fault: implications for wrench tectonics. Geology 15, 1143–1146.
Panza, G.F., Raykova, R., 2008. Structure and rheology of lithosphere in Italy and surrounding. Terra Nova 20, 194–199.
Panza, G.F., Pontevivo, A., Chimera, G., Raykova, R., Aoudia, A., 2003. The lithosphere–asthenosphere: Italy and surroundings. Episodes-Newsmagazine of the International Union of Geological Sciences 26, 169–174.
Pasquale, V., Cabella, C., Verdoya, M., 1990. Deep temperatures and lithospheric thickness along the European Geotraverse. Tectonophysics 176, 1–11.
Peltzer, G., Tapponnier, P., Zhang, Z.T., Xu, Z.Q., 1985. Neogene and Quaternary faulting in and along the Qinling Shan. Nature 317 (6037), 500–505.
Pérez-Gussinyé, M., Lowry, A.R., Watts, A.B., 2007. Effective elastic thickness of South America and its implications for intracontinental deformation. Geochemistry, Geophysics, Geosystems 8, Q05009. http://dx.doi.org/10.1029/2006GC001511.
Pérez-Gussinyé, M., Metois, M., Fernández, M., Vergés, J., Fullea, J., Lowry, A.R., 2009. Effective elastic thickness of Africa and its relationship to other proxies for lithospheric structure and surface tectonics. Earth and Planetary Science Letters 287 (1–2), 152–167.
Ranalli, G., 1997. Rheology of the lithosphere in space and time. Geological Society, London, Special Publications 121 (1), 19–37.
Rybach, L., Buntebarth, G., 1984. The variation of heat generation, density and seismic velocity with rock type in the continental lithosphere. Tectonophysics 103, 335–344.
Salon, S.A., 1977. Major tectonic characteristics and development history of the Sichote-Aline fold systems. Geotectonics 1, 51–78.
Scott, R.W., Wan, X., Wang, C., Huang, Q., 2012. Late Cretaceous chronostratigraphy (Turonian-Maastrichtian): SK1 core Songliao Basin, China. Geoscience Frontiers 3, 357–367.
Tao, W., Shen, Z., 2008. Heat flow distribution in Chinese continent and its adjacent areas. Progress in Natural Science 18, 843–849.
Tapponnier, P., Molnar, P., 1977. Active faulting and tectonics in China. Journal of Geophysical Research 82 (20), 2905–2930.
Teng, J.W., Wang, Q.S., Liu, Y.L., Wei, S.S., 1983. The characteristics of geophysical field and the distribution and formation of oil and gas bearing basin in eastern China. Chinese Journal of Geophysics 26 (4), 319–330 (in Chinese with English abstract).
Teng, J.W., Wang, G.J., Zhang, Z.J., Hu, J.F., 2001. The 3-D structure of shear wave in South China and the southward extension of Tanlu fault. Chinese Science Bulletin 46 (4), 284–289 (in Chinese with English abstract).
Teng, J.W., Yan, Y.F., Wang, G.J., Xiong, X., 2006. Structure of Earth's crust and upper mantle, inland subduction and its coupling effects on the Dabie orogenic belt and the Tancheng-Lujiang fault zone. Chinese Journal of Geophysics 49 (2), 449–457 (in Chinese with English abstract).
Thybo, H., Nielsen, C.A., 2009. Magma-compensated crustal thinning in continental rift zones. Nature 457, 873–976. http://dx.doi.org/10.1038/nature07688.
Thybo, H., Maguire, P.K.H., Birt, C., Perchuc, E., 2000. Seismic reflectivity and magmatic underplating beneath the Kenya Rift. Geophysical Research Letters 27 (17), 2745–2748.
Thybo, H., Sandrin, A., Nielsen, L., Lykke-Andersen, H., Keller, G.R., 2006. Seismic velocity structure of a large mafic intrusion in the crust of central Denmark from project ESTRID. Tectonophysics 420, 105–122.
Tian, Y., Zhao, D., 2011. Destruction mechanism of the North China Craton: Insight from P and S wave mantle tomography. Journal of Asian Earth Sciences 42 (6), 1132–1145.
Tian, Y., Zhao, D., Sun, R., Teng, J.W., 2009. Seismic imaging of the crust and upper mantle beneath the North China Craton. Physics of the Earth and Planetary Interiors 172, 169–182.
Uyeda, S., Kanamori, H., 1979. Back-arc opening and the mode of subduction. Journal of Geophysical Research 84 (3), 1049–1061.
Uyeda, S., Miyashiro, A., 1974. Plate tectonics and the Japanese Islands: a synthesis. Bulletin of the Geological Society of America 85 (7), 1159–1170.
Waldhauser, F., Ellsworth, W.L., 2000. A double-difference earthquake location algorithm: method and application to the northern Hayward fault. California. Bulletin of the Seismological Society of America 90 (6), 1353–1368.
Wan, T.F., Zhu, H., Zhao, L., Lin, J.P., Chen, J., Chen, J., 1996. Formation and evolution of the Tancheng-Lujiag fault zone: a review. Geoscience 10 (2), 159–168 (in Chinese with English abstract).
Wang, Y., 2001. Heat flow pattern and lateral variations of lithosphere strength in China mainland: constraints on active deformation. Physics of the Earth and Planetary Interiors 126 (3–4), 121–146.
Wang, Y.J., Cheng, S.X., 1992. A type overthrusting of Tancheng-Lujiang fault zone (the Jiashan-Lujiang sector). Regional Geology of China 3, 241–247 (in Chinese with English abstract).
Wang, W.F., Jin, Q., Ma, Z.J., 1998. Meso-Cenozoic Evolution of the Tanlu fault and formation of sedimentary basins. Acta Geologica Sinica-English Edition 72 (4), 350–362.

Wang, C.Y., Zeng, R.S., Mooney, W.D., Hacker, B.R., 2000. A crustal model of the ultrahigh-pressure Dabie Shan orogenic belt, China, derived from deep seismic refraction profiling. Journal of Geophysical Research 105 (B5), 10857–10869.
Wang, S.Y., Hearn, T.M., Xu, Z.W., Ni, J.F., Yu, Y.X., Zhang, X.D., 2001. Pn wave velocity structure at the uppermost mantle of China. Science in China (Series D) 31 (6), 449–454 (in Chinese).
Wang, X.Y., Zhu, W.Y., Fu, Y., You, X.Z., Wang, Q., Cheng, Z.Y., Ren, J.W., 2002. Present-time crustal deformation in China and its surrounding regions by GPS. Chinese Journal of Geophysics 45 (2), 198–209 (in Chinese with English abstract).
Watts, A.B., 2001. Isostasy and Flexure of the Lithosphere. Cambridge University Press, Cambridge, pp. 176–221.
Watts, A.B., Burov, E.B., 2003. Lithospheric strength and its relationship to the elastic and seismogenic layer thickness. Earth and Planetary Science Letters 213 (1–2), 113–131.
Wu, J., Zhang, Z.J., 2012. Spatial distribution of seismic layer, crustal thickness, and Vp/Vs ratio in the Permian Emeishan Mantle Plume region. Gondwana Research 22 (1), 127–139. http://dx.doi.org/10.1016/j.gr.2011.10.007.
Wu, F.Y., Walker, R.J., Ren, X.W., Sun, D.Y., Zhou, X.H., 2003. Osmium isotopic constrains on the age of lithospheric mantle beneath northeastern China. Chemical Geology 196, 107–129.
Wu, F.Y., Yang, J.H., Wilde, S.A., Zhang, X.O., 2005. Geochronology, petrogenesis and tectonic implications of Jurassic granites in the Liaodong Peninsula, NE China. Chemical Geology 221 (1), 127–156.
Wu, F.Y., Walker, R.J., Yang, Y.H., Yuan, H.L., Yang, J.H., 2006. The chemical-temporal evolution of lithospheric mantle underlying the North China Craton. Geochemica et Cosmochimica Acta 70, 5013–5034.
Xiao, Y., Zhang, H.F., 2011. Effects of melt percolation on platinum group elements and Re-Os systematics of peridotites from the Tan-Lu fault zone, eastern North China Craton. Journal of the Geological Society 168, 1201–1214.
Xiao, Y., Zhang, H.F., Fan, W.M., Ying, J.F., Zhang, J., Zhao, X.M., Su, B.X., 2010. Evolution of lithospheric mantle beneath the Tan-Lu fault zone, eastern North China Craton: evidence from petrology and geochemistry of peridotite xenoliths. Lithos 17 (1), 229–246.
Xu, J.W., 1984a. The Slip Fault System of Tanlu. Papers of Tectonic Geology, China. Geological Publishing House, Beijing, pp. 18–33.
Xu, Z.Q., 1984b. Papers of Tectonic Geology, China. Geological Publishing House, Beijing, pp. 39–46.
Xu, J.W., Zhu, G., 1995. Discussion on tectonic model for the Tanlu fault zone, eastern China. Journal of Geological Miner Research North China 10 (2), 121–134 (in Chinese with English abstract).
Xu, J.W., Zhu, G., Tong, W., Cui, K., Liu, Q., 1987. Formation and evolution of the Tancheng-Lujiang wrench fault system: a major shear system to the northwest of the Pacific Ocean. Tectonophysics 134 (4), 273–310.
Xu, J.W., Ma, G.F., Tong, W.X., Zhu, G., Lin, S.F., 1993. Displacement of the Tancheng-Lujiang wrench fault system and its geodynamic setting in the northwestern circum-Pacific. In: Xu, J.W. (Ed.), The Tancheng-Lujiang Wrench Fault System. John Wiley and Sons Ltd., pp. 51–74.
Xu, X.S., O'Reilly, S.Y., Griffin, W.L., Zhou, X.M., Huang, X.L., 1998. The nature of the cenozoic lithosphere at Nüshan, Eastern China. In: Flower, M.F.J., Chung, S.J., Lo, C.H., Lee, T.Y. (Eds.), Mantle Dynamics and Plate Interactions in East Asia: American Geophysical Union, Geodynamics Series, pp. 167–195.
Xu, Y., Li, Z.W., Huang, R.Q., Liu, J.H., Liu, J.S., 2010. Pn-wave velocity and anisotropy of the western Sichuan and Longmen Mountain region, China. Science in China (Series D) 53 (11), 1665–1670.
Xu, W.L., Zhou, Q.J., Pei, F.P., Yang, D.B., Gao, S., Li, Q.L., Yang, Y.H., 2012. Destruction of the North China Craton: Delamination or thermal/chemical erosion? Mineral chemistry and oxygen isotope insights from websterite xenoliths. Gondwana Research. <http://dx.doi.org/10.1016/j.gr.2012.02.008>.
Yang, B.J., Mu, S.M., Jin, X., Liu, C., 1996. Synthesized studies on the geophysics of the Manzhouli–Suifenhe geoscience transect, China. Chinese Journal of Geophysics 36 (6), 772–782 (in Chinese with English abstract).
Yang, W., Qu, C., Yu, C., 2011. Crustal Poisson's ratio anomalies in the eastern part of North China and their origins. Geoscience Frontiers 2, 313–321.
Yang, K.F., Fan, H.R., Santosh, M., Hu, F.F., Wilde, S.A., Lan, T.G., Lu, L.N., Liu, Y.S., 2012. Reactivation of the Archean lower crust: implications for zircon geochronology, elemental and Sr–Nd–Hf isotopic geochemistry of Late Mesozoic granitoids from northwestern Jiaodong Terrane, North China Craton. Lithos 146–147, 112–127.
Ye, H., Zhang, B., Mao, F., 1987. The Cenozoic tectonic evolution of the Great North China: two types of rifting and crustal necking in the Great North China and their tectonic implications. Tectonophysics 133 (3), 217–227.
Ye, G.F., Wei, W.B., Jin, S., Jing, J.E., 2009. Study of the electrical structure and its geological meanings of the middle part of Tancheng-Lujiang fault zone. Chinese Journal of Geophysics 52 (11), 2818–2825 (in Chinese with English abstract).
Yin, A., 2010. Cenozoic tectonic evolution of Asia: a preliminary synthesis. Tectonophysics 488 (1–4), 293–325.
Yin, A., Nie, S., 1993. An indentation model for the North and South China collision and the development of the Tan-Lu and Honam fault systems, eastern Asia. Tectonics 12 (4), 801–813.
Ying, J.F., Zhang, H.F., Kita, N., Morishita, Y., Shimoda, G., 2006. Nature and evolution of late cretaceous lithospheric mantle beneath the eastern North China Craton: constraints from petrology and geochemistry of peridotitic xenoliths from Junan, Shandong Province, China. Earth and Planetary Science Letters 244, 622–638.
Zang, S.X., Liu, Y.G., Ning, J.Y., 2002. Thermal structure of the lithosphere in North China. Chinese Journal of Geophysics 45 (1), 56–66 (in Chinese with English abstract).
Zeng, G., Chen, L.H., Hofmann, A.W., Jiang, S.Y., Xu, X.S., 2011. Crust recycling in the sources of two parallel volcanic chains in Shandong, North China. Earth and Planetary Science Letters 302, 359–368.
Zhai, M.G., Santosh, M., 2011. The early Precambrian odyssey of the North China Craton: a synoptic overview. Gondwana Research 20, 6–25.
Zhang, H.F., 2009. Peridotite-melt interaction: a key point for the destruction of cratonic lithospheric mantle. Chinese Science Bulletin 54 (19), 3417–3437.
Zhang, H.F., 2012. Destruction of ancient lower crust through magma underplating beneath Jiaodong Peninsula, North China Craton: U-Pb and Hf isotopic evidence from granulite xenoliths. Gondwana Research 21, 281–292.
Zhang, J., Zhang, H.F., 2007. Compositional features and P–T conditions of granulite xenoliths from late Cretaceous mafic dike, Qingdao region. Acta Petrologica Sinica 23, 1133–1140 (in Chinese with English abstract).
Zhang, Z.M., Liou, J.G., Coleman, R.G., 1984. An outline of the plate tectonics of China. Bulletin of the Geological Society of America 95 (3), 295–312.
Zhang, Y.Q., Vergely, P., Mercier, J., 1995. Active faulting in and along the Qinling Range (China) inferred from imagery analysis and extrusion tectonics of south China. Tectonophysics 243 (1–2), 69–95.
Zhang, Y.Q., Mercier, J.L., Vergély, P., 1998. Extension in the graben systems around the Ordos (China), and its contribution to the extrusion tectonics of south China with respect to Gobi-Mongolia. Tectonophysics 285 (1–2), 41–75.
Zhang, Z.J., Li, Y.K., Lu, D.Y., Wang, G.J., Teng, J.W., 2000. Velocity and anisotropy structure of the crust in the Dabieshan orogenic belt from wide-angle seismic data. Physics of the Earth and Planetary Interiors 122 (1–2), 115–131.
Zhang, Y.Q., Dong, S., Shi, W., 2003a. Cretaceous deformation history of the middle Tan-Lu fault zone in Shandong Province, eastern China. Tectonophysics 363 (3–4), 243–258.
Zhang, H.F., Sun, M., Zhou, X.H., Zhou, M.F., Fan, W.M., Zheng, J.P., 2003b. Secular evolution of the lithosphere beneath the eastern North China Craton: evidence from Mesozoic basalts and high-Mg andesites. Geochimica et Cosmochimica Acta 67 (22), 4373–4387.
Zhang, Z.J., Badal, J., Li, Y.K., Chen, Y., Yang, L.Q., Teng, J.W., 2005. Crust-upper mantle seismic velocity structure across Southeastern China. Tectonophysics 395 (1–2), 137–157. http://dx.doi.org/10.1016/j.tecto.2004.08.008.
Zhang, P., Wang, L.S., Zhong, K., Ding, Z.Y., 2007. Research on the segmentation of the Tancheng-Lujiang Fault Zone. Geological Review 53 (5), 586–593 (in Chinese with English abstract).
Zhang, Z.J., Zhang, X., Badal, J., 2008. Composition of the crust beneath southeastern China derived from an integrated geophysical data set. Journal of Geophysical Research 113, B04417. http://dx.doi.org/10.1029/2006JB004503.
Zhang, Z.J., Bai, Z.M., Mooney, W., Wang, C.Y., Chen, X.B., Wang, E.C., Teng, J.W., Okaya, N., 2009. Crustal structure across the three gorges area of the Yangtze platform, central China, from seismic refraction/wide-angle reflection data. Tectonophysics 475 (3–4), 423–437.
Zhang, H.F., Zhou, M.F., Sun, M., Zhou, X.H., 2010a. The origin of Mengyin and Fuxian diamondiferous kimberlites from the North China Craton: Implication for Palaeozoic subducted oceanic slab-mantle interaction. Journal of Asian Earth Sciences 37 (5–6), 425–437.
Zhang, J.H., Zhao, G.Z., Xiao, Q.B., Tang, J., 2010b. Analysis of electric structure of the central Tan-Lu fault zone (Yi-Shu fault zone, 36°N) and seismogenic condition. Chinese Journal of Geophysics 53 (3), 605–611 (in Chinese with English abstract).
Zhang, H.F., Ying, J.F., Tang, Y.J., Li, X.H., Feng, C., Santosh, M., 2011a. Phanerozoic reactivation of the Archean North China Craton through episodic magmatism: evidence from zircon U-Pb geochronology and Hf isotopes from the Liaodong Peninsula. Gondwana Research 19, 446–459.
Zhang, J., Zhang, H., Kita, N., Shimoda, G., Morishita, Y., Ying, J., Tang, Y., 2011b. Secular evolution of the lithospheric mantle beneath the eastern North China Craton: evidence from peridotitic xenoliths from Late Cretaceous mafic rocks in the Jiaodong region, east-central China. International Geology Review 53 (2), 182–211.
Zhang, Z.J., Yang, L., Teng, J., Badal, J., 2011c. An overview of the earth crust under China. Earth-Science Reviews 104 (1–3), 143–166.
Zhang, Z.J., Chen, Q.F., Bai, Z.M., Chen, Y., Badal, J., 2011d. Crustal structure and extensional deformation of thinned lithosphere in Northern China. Tectonophysics 508 (1–4), 62–72. http://dx.doi.org/10.1016/j.tecto.2010.06.021.
Zhang, Z.J., Klemperer, S.L., Bai, Z.M., Chen, Y., Teng, J.W., 2011e. Crustal structure of the Paleozoic Kunlun orogeny from an active-source seismic profile between Moba and Guide in East Tibet, China. Gondwana Research 19 (4), 994–1007. http://dx.doi.org/10.1016/j.gr.2010.09.008.
Zhang, Z.J., Wu, J., Deng, Y., Teng, J., Chen, Y., Panza, G., 2012a. Lateral variation of strength of the lithosphere across the eastern North China Craton: new constraints on lithospheric disruption. Gondwana Research 22 (3–4), 1047–1059. http://dx.doi.org/10.1016/j.gr.2012.03.006.
Zhang, Z.J., Deng, Y.F., Chen, L., Wu, J., Teng, J.W., Panza, G., 2012b. Seismic structure and rheology of the crust beneath mainland China. Gondwana Research. http://dx.doi.org/10.1016/j.gr.2012.07.010.
Zhao, L., Allen, R.M., Zheng, T.Y., Huang, S.F., 2009a. Reactivation of an Archean craton: constraints from P-and S-wave tomography in North China. Geophysical Research Letters 36, L17306. http://dx.doi.org/10.1029/2009GL039781.

Zhao, D., Tian, Y., Lei, J., Liu, L., Zheng, S., 2009b. Seismic image and origin of the Changbai intraplate volcano in East Asia: role of big mantle wedge above the stagnant Pacific slab. Physics of the Earth and Planetary Interiors 173, 197–206.

Zheng, Y., Teng, J.W., 1989. The structure of the crust and upper mantle in the Shuixian-Maanshan zone and some charateristic of the south part of the Tan-Lu tectonic belt. Chinese Journal of Geophysics 32, 648–659 (in Chinese with English abstract).

Zheng, J.P., O'Reilly, S.Y., Griffin, W.L., Lu, F.X., Zhang, M., 1998. Nature and evolution of Cenozoic lithospheric mantle beneath the Shandong peninsula, Sino-Korean Craton, eastern China. International Geology Review 40, 471–499.

Zheng, J.P., O'Reilly, S.Y., Griffin, W.L., Lu, F.X., Zhang, M., Pearson, N.J., 2001. Relict refractory mantle beneath the eastern North China block: significance for lithosphere evolution. Lithos 57, 43–66.

Zheng, T.Y., Chen, L., Zhao, L., Xu, W.W., Zhu, R.X., 2006. Crust–mantle structure difference across the gravity gradient zone in North China Craton: seismic image of the thinned continental crust. Physics of the Earth and Planetary Interiors 159 (1), 43–58.

Zheng, T.Y., Chen, L., Zhao, L., Zhu, R.X., 2007a. Crustal structure across the Yanshan belt at the northern margin of the North China Craton. Physics of the Earth and Planetary Interiors 161 (1), 36–49.

Zheng, J.P., Griffin, W.L., O'Reilly, S.Y., Yu, C.M., Zhang, H.F., Pearson, N., Zhang, M., 2007b. Mechanism and timing of lithospheric modification and replacement beneath the eastern North China Craton: peridotitic xenoliths from the 100 Ma Fuxin basalts and a regional synthesis. Geochimica et Cosmochimica Acta 71, 5203–5225.

Zheng, J.P., Griffin, W.L., O'Reilly, S.Y., Hu, B.Q., Zhang, M., Tang, H.Y., Su, Y.P., Zhang, Z.H., Pearson, N., Wang, F.Z., Lu, F.X., 2008. Continental collision and accretion recorded in the deep lithosphere of central China. Earth and Planetary Science Letters 269 (3), 497–507.

Zhu, R.X., Zheng, T.Y., 2009. Destruction geodynamics and Paleoproterozoic plate tectonics of the North China Craton. Chinese Science Bulletin 54 (14), 1950–1961.

Zhu, G., Song, C.Z., Wang, D.X., Liu, G.S., Xu, J.W., 2001a. Studies on $^{40}Ar/^{39}Ar$ thermochronology of strike-slip time of the Tan-Lu fault zone and their tectonic implications. Science in China (Series D) Earth Sciences 44 (11), 1002–1009.

Zhu, G., Wang, D.X., Liu, G.S., Song, C.Z., Niu, M.L., Xu, J.W., 2001b. Extensional activities along the Tanlu Fault zone and its geodynamic setting. Chinese Journal of Geology 36 (3), 269–278 (in Chinese with English abstract).

Zhu, G., Song, C.Z., Niu, M.L., Liu, G.S., Wang, Y.S., 2002. Lithospheric textures of the Tan-lu Fault Zone and their genetic analysis. Geological Journal of China Universities 8 (3), 248–256 (in Chinese with English abstract).

Zhu, G., Wang, D.X., Liu, G.S., Niu, M.L., Song, C.Z., 2004. Evolution of the Tan-lu fault zone and its responses to plate movement in west Pacific basin. Chinese Journal of Geology 39 (1), 36–49 (in Chinese with English abstract).

Zhu, G., Niu, M.L., Liu, G.S., Wang, Y.S., Xie, C.L., Li, C.C., 2005. $^{40}Ar/^{39}Ar$ dating for the strike-slip movement on the Feidong part of Tan-lu fault belt. Acta Geological Sinica 79 (3), 303–316 (in Chinese with English abstract).

Zhu, G., Jiang, D., Zhang, B., Chen, Y., 2012. Destruction of the eastern North China Craton in a backarc setting: Evidence from crustal deformation kinematics. Gondwana Research 22 (1), 86–103.

Zu, J.H., Wu, Q.F., Lian, Y.F., 1996. Geothermal study of the mid-segment of the Tancheng-Lujiang fault zone and its neighboring region. Earthquake Research in China 12 (1), 43–48 (in Chinese with English abstract).